



Research

# Simplified numerical model development for advanced design of lightweight-concrete encased cold-formed steel shear wall panels

Nathalie Eid<sup>1</sup>  · Attila László Joó<sup>1</sup> 

Received: 28 August 2023 / Accepted: 10 November 2023

Published online: 24 November 2023

© The Author(s) 2023 [OPEN](#)

## Abstract

Since cold-formed steel (CFS) elements are susceptible to complex buckling phenomena that decrease their structural capability, many strengthening trends have been developed so far. One of these methods is the use of polystyrene aggregate concrete (PAC) as bracings in order to restrain the global and distortional buckling modes of CFS members, where a new structural system comprising CFS elements encased in PAC has been proposed. In this research, PAC-encased CFS shear panels have been investigated numerically, where a simplified finite element model was developed to predict the structural behavior and capacity of such members. This goal was achieved using ANSYS software, where a geometrically and materially nonlinear analysis with imperfections (GMNI) was used to solve the problem of PAC-encased CFS shear panels. The full detailed volume-contact element-based concrete model was replaced by spring elements perpendicular to the plate's plane with equivalent properties, and beam elements that could represent the concrete block more accurately regarding the global lateral stiffness and shear resistance. Consequently, for this case, the combination of local and global stiffness of PAC could produce the actual shear behavior of PAC-filled wall panels. The developed model was validated against previous experimental tests from the literature. Parametric studies were conducted in terms of the imperfection amplitudes, the stiffness of springs and the properties of PAC. Finally, the structural performance of PAC-encased panels under combined axial and shear loading was examined, where the effect of different axial load levels on the lateral strength was determined, and an interaction equation was proposed.

## Article Highlights

- An innovative simplified numerical model was developed to predict the shear performance of PAC-encased CFS wall panels.
- The effect of different imperfection amplitudes and PAC properties on the shear performance of PAC-encased CFS walls were investigated.
- An interaction curve was proposed to predict the resistance of PAC-filled CFS walls under combined vertical and shear action.

**Keywords** Cold-formed steel · Structural stability · Polystyrene aggregate concrete · Nonlinear finite element analysis · Shear resistance of PAC-encased CFS panels · Compression-shear interaction resistance of PAC-encased CFS panels

✉ Nathalie Eid, [Nathalie.eid@edu.bme.hu](mailto:Nathalie.eid@edu.bme.hu), <https://epito.bme.hu/eid-nathalie?language=en>; Attila László Joó, [joo.attila@emk.bme.hu](mailto:joo.attila@emk.bme.hu), <https://epito.bme.hu/node/11436?language=en> | <sup>1</sup>Department of Structural Engineering, Faculty of Civil Engineering, Budapest University of Technology and Economics, Műegyetem rkp. 3, 1111 Budapest, Hungary.



SN Applied Sciences

(2023) 5:366

| <https://doi.org/10.1007/s42452-023-05590-7>

SN Applied Sciences  
A **SPRINGER NATURE** journal

## 1 Introduction

### 1.1 Background of the research

As a feasible structural technology, CFS constructions are often used in residential, commercial, and public buildings. That is due to the benefits of CFS elements, such as lightweight, high strength, rapid installation, and efficient transportation.

Two major manufacturing procedures are being used at room temperature to form CFS members: cold-rolling and press braking. Due to the forming process, strain hardening at the plastic zones (mainly corner zones) occurs. Compared with hot-rolled members, more variety of cross-section shapes can be formed due to the straightforward manufacturing process. Hence, profile optimization, including the formation of internal and edge stiffeners within the cross-section that give full or partial restraint to the stiffened plates, can play a crucial role in this sector by enhancing their load-bearing capacities. These thin-walled elements usually have a zinc coat layer for protection from corrosion.

Two key elements in the features and design concepts of CFS sections are their large width-to-thickness ratio and small torsional rigidity since the maximum thickness is around 4 mm and the cross-sections are mostly open. Consequently, these elements are prone to various complex types of buckling, such as global, distortional, local and other interactive buckling modes that modify the stress distribution and decrease their bearing capacity. The most common shapes of the open forms of CFS sections, especially those used in structural framing, are channels (C-sections), angles, Z-sections, hat sections, T-sections and I-sections. Additionally, imperfections; that appear in the manufacturing process or during the construction phase, are also a critical factor in the design considerations of CFS elements. Equivalent imperfections in design specifications mean that the applied imperfection should consider the effect of all kinds of imperfections. In addition, the current design rules are not applicable to all configurations and connection types; thus, the test-based design approach allows the calculation of design resistances for specific tests that are measured in laboratories and still provides the necessary safety level for design purposes. Additionally, the development of the actual design methods in standards can be done based on the observations of test-based design calculations, where nonconservative design methods may be derived and consequently reduce the construction cost of structures.

On the other hand, virtual tests using advanced numerical methods (FEM) are an alternative way to

estimate the design capacity of members with a particular structural arrangement that are not specified within the existing standards. These inexpensive tools are able to accurately simulate and analyze the possible buckling types and failure modes that occur in cold-formed steel members by choosing the appropriate software, element types, boundary conditions, buckling modes with appropriate imperfections, material properties and finally by applying Geometric and Material Nonlinear Analysis with Imperfections (GMNI analysis).

However, various stability phenomena that occur in this type of structures decrease their bearing strength. Hence, a variety of strengthening strategies have been suggested recently. Namely, using PAC as infill substance, which performs as continuous bracing for load-bearing components, is one of these methods. One of the research projects that suggested and contributed to the development of this approach was conducted in Hungary by Hegyi and Dunai [1]. This paper will continue the previous work, where more details about the analyzed structural system, problem statement and aim of the current research are discussed in the following subsections.

### 1.2 Structural arrangement of the proposed system

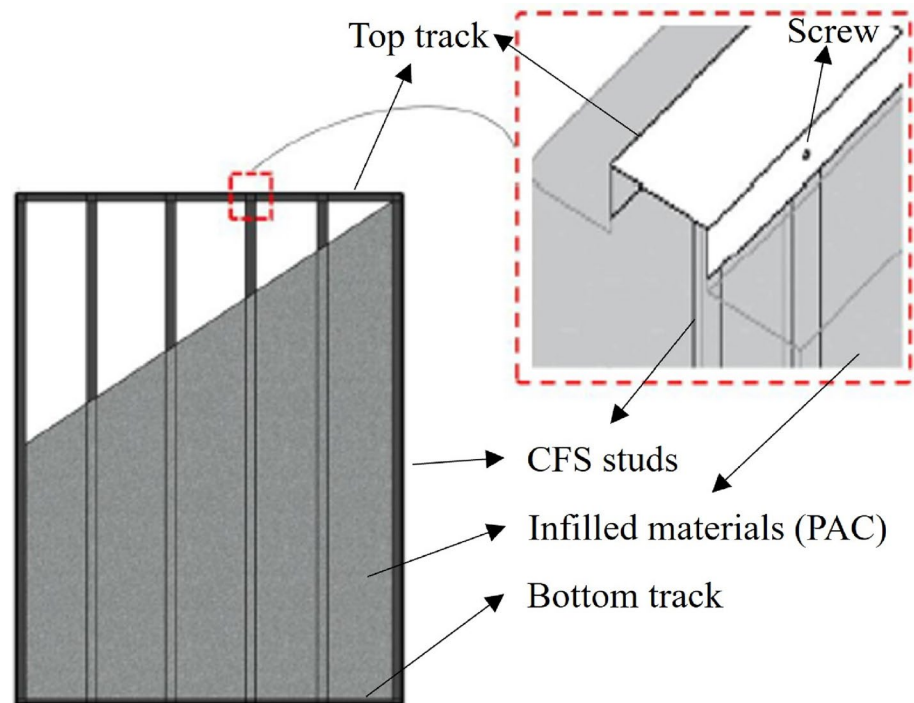
The system is composed of precast panel components. The first part is represented by the steel core of panels, which consists of channel-profiled elements that are assembled with U-profiled tracks at the top and bottom by self-drilling screws. The panels are then created by casting the concrete. Finally, gusset plates and self-drilling screws are used to join panels to each other in situ, where the outside edge zone of the top and bottom tracks have to stay PAC-free in order to establish these connections, as depicted in Fig. 1.

The type of concrete which was used here is polystyrene aggregate concrete. It has a foam-like behavior with a low modulus of elasticity, and great deformation capacity, which varies between 30 and 200 MPa, while its compressive strength can be as low as 0.1 MPa and up to 0.25 MPa and the flexural strength varies between 0.044 and 0.199 MPa. Thus, it is unsuitable for structural load-bearing applications; however, it could be used efficiently as a filling and insulation material due to its lightweight and low thermal conductivity.

### 1.3 Problem statement

In fact, a new building system will be produced by using this new type of cold-formed steel elements encased with PAC. Thus, this new system should be checked experimentally as well as numerically. Additionally, the previous research works showed that the current rules and

**Fig. 1** Structural arrangement of PAC-encased CFS panels



regulations of the available CFS standard (Eurocode 1993-1-3 [2]) are not applicable to the new structural systems and hence, it is necessary to develop new design specifications for the proposed cold-formed and thin-walled steel systems. Thus, numerous expensive experimental tests and numerical simulations have to be carried out within the framework of this development.

On the other hand, modeling the full detailed volume-contact elements-based part of the solid concrete block, including the exact material model of concrete and the shell-contact elements-based part of steel elements in such advanced structural systems, might be quite difficult and complicated. Even though the entire model for similar structures was conducted in some research works, which will be mentioned in Sect. 2, the modeling procedure would be time-consuming, computationally expensive and unsuitable for practical cases, especially if the whole building has to be modeled and analyzed by GMNI analysis.

#### 1.4 Solution, scope and methodology

The main purpose of the present research work is to develop a simplified finite element model of PAC-encased CFS elements; in order to avoid the obstacles and toughness of modeling the concrete part along with the interaction surfaces with steel, by substituting the volume and contact elements with equivalent spring and beam elements. This simplified model can be applied by practicing engineers without the need to perform a complicated one

and can be used later to expand the data of experiments and to develop new design formulae for PAC-encased thin-walled steel members. If a complex modeling and design method were available, it would help the spread of an innovative structural system, creating new ways of construction for residential buildings and other functions.

In fact, the current work is the continuation of the research study that was conducted by Hegyi and Dunai [1], where the system was proposed, and an extensive test program was carried out. Some parts of this experimental program will be detailed in Sect. 3. For the current study, columns, connections and wall panels under axial load have already been modeled, where the simplified model was introduced and developed [3] 4. In this paper, the PAC-encased CFS wall panels under the following loading conditions will be investigated:

- Wall panels under shear load (Sect. 3).
- Wall panels under combined action of compression and shear (Sect. 4).

Indeed, a special modeling technique was proposed and verified by the available test results. PAC was replaced by springs that are perpendicular to the plate's plane with specific properties. Additionally, a new beam element has been introduced that could represent the concrete block more accurately in terms of the global lateral stiffness and shear resistance provided by PAC and connected by rigid region means with the shell and spring elements. Consequently, the combination of local and global stiffness

of PAC could produce the actual shear behavior of PAC-filled wall panels. After that, test-based design values were evaluated based on Eurocode [2] and numerical design values were obtained using nominal material properties and dimensions. This model was further used to investigate the structural performance of PAC-encased panels under combined vertical and shear loading, where the effect of different axial load levels on the lateral strength and stiffness of walls was determined, and an interaction equation was proposed in Sect. 4. Finally, conclusions were drawn in Sect. 5.

Consequently, this research study suggests a simplified practical manner for the modeling and simulation of PAC-encased CFS elements. The applied method is a kind of FEM-based design approach, where GMNI analysis will be used to follow the behavior of PAC-encased thin-walled steel elements. Furthermore, the framework which is presented in this paper is an essential tool for later numerical investigations in this field.

## 2 Literature review

The lateral resistance of CFS constructions is generally provided by CFS framed walls, mainly through sheathings, infill materials or bracing systems. One of the sheathing substances is thin steel plates, which increase the panel's lateral strength and enhance the structure's ductility and ability to dissipate energy. For example, Zhang et al. [5] investigated high-strength CFS framed shear walls along with steel sheets. They used two approaches to enhance the shear capacity. The first one was using higher thickness for studs and tracks, and the second one was increasing the number of screws for the sheathing.

Similarly, Attari et al. [6] performed experimental and numerical studies on CFS shear panels. The tested walls had one or two sheets where reversed cyclic loading was applied. However, monotonic pushover loading was used in the numerical analysis. Specifically, lateral load-story drift, ultimate strength and failure types of the walls were examined. The outcomes revealed that the thickness considerably affects the resistance. A linear relationship was also detected between the ratio of ultimate capacity to frame thickness, and the sheet thickness, and the results were compared with those obtained from AISI S213 code.

On the other hand, Xu et al. [7] developed an improved system of CFS shear panels by using high-strength lightweight concrete as a filling substance with straw boards. Different failure modes occurred in the foamed concrete and studs, which were characterized as ductile failure. They concluded that the stiffness was boosted up to 4.6 times by increasing the wall thickness and density grade of the concrete. Finally, they proposed a design formula to

predict the shear capacity of these walls. Likewise, straw-bale was also used as a filling material for CFS shear panels in China. This solution aims to reduce the straw removal issue, carbon emissions and building heating energy. Namely, Chen et al. [8] proposed an enhanced CFS walls system by using a built-in straw-bale along with welded-wire-mesh-cement-mortar sheathing. They determined the appropriate screws configuration, degree of straw-bale compaction, welded-wire diameter and cement mortar strength. In the same way, Wu et al. [9] examined wall panels infilled with flue gas desulfurization (FGD) gypsum under shear action in order to improve the shear behavior. The detected failure modes were a compressive failure of gypsum, where the infilled gypsum was divided into several pieces by CFS studs, a compressive failure occurred in the corner of each piece, and stressed skin of sheathing. They also estimated the lateral stiffness of the investigated walls based on superposition methods and failure modes within the same research framework [10]. The shear stiffness of screws was also estimated through a theoretical method in order to define the influence of sheathings on the lateral stiffness. Wang et al. [11] analyzed the cyclic performance of CFS wall panels infilled with lightweight polymer material (LPM) under shear action. Different failure types were detected during tests, such as local and distortional buckling of columns, tilting of sheathing screws, and crushing of LPM. In the same way, Hegyi and Dunai [1] examined the performance of Channel CFS wall panels encased in PAC under shear action. In this research paper, the results of their experimental program will be implemented in the validation of the developed numerical model, where more information about this program is detailed in Sect. 3.

Hu et al. [12] proposed an innovative system of CFS walls to enhance their seismic performance and shear capacity using phosphogypsum (PG) as a filling substance. The wall was filled with phosphogypsum in and between the studs, which were steel tubes. This system was investigated experimentally under cyclic lateral loads considering different PG strength, axial compression ratio and the steel tube's wall thickness. The outcomes indicate that the wall thickness of steel tubes and the axial compression ratio have a considerable impact on the seismic performance of the composite walls, while the PG strength has a smaller influence on the seismic behavior. They also suggested calculation formulae and an analytical model for predicting the shear capacity of PG-filled CFS walls. A similar study was conducted by Yin et al. [13] to examine the effect of phosphogypsum filling on the axial compression behavior of CFS walls. The outcomes revealed that the axial bearing capacity increased by 115.7%, where the detected failure modes were buckling of the steel tubes, distorting of tracks, and crushing of PG.

Apart from that, Usefi et al. [14] improved the shear resistance of CFS panels through introducing a new hybrid system that consists of square hollow sections truss in addition to CFS open sections, where different configurations and connection details were tested. This solution provided a significant lateral resistance and energy absorption with relatively low weight in comparison with infilled walls, especially by applying the truss to one side of the panels.

Few examples in the literature were conducted on the behavior of CFS wall panels under combined vertical and lateral loading. One of them was carried out by Yilmaz et al. [15] who investigated numerically the impact of different gravity loading intensity levels on the lateral behavior of CFS panels with oriented strand board sheathing. The outcomes revealed that high vertical load ratios (around 60% of the total compressive capacity) have the ability to severely decrease the lateral resistance, energy dissipation and ductility due to the premature local buckling of studs under axial action, whereas the impact of vertical loads on the initial stiffness of the system was negligible. Similarly, another numerical investigation [16] was done for CFS strap-braced walls under axial and lateral loading, where the lateral capacity and ductility corresponding to different vertical loading levels were estimated by deriving specific formulae. The findings showed that vertical loading can significantly decrease the ductility and ultimate displacement of the panels. Hence, a suitable design methodology was also suggested, taking into account the presence of axial loads in the shear analysis of such components in order to achieve the desired seismic loading and ductility. The maximum gravity loading ratio that was used in this study was 58% of the total compressive capacity of the studs, that caused a drop of more than 70% in terms of ductility and displacement values. While for strap thicknesses greater than 1.11 mm and up to 2.22 mm, a 51% gravity loading ratio could reduce the ductility and ultimate displacement by more than 85% due to an already greater axial force on the chord. However, for strap thicknesses higher than 2.77 mm the ductility value was below 2.5 that is unsuitable for seismic applications. This emphasizes the significance of taking into account the impacts of gravity loading in the seismic analysis of similar systems.

Similarly, Ayatollahi et al. [17] examined the lateral structural behavior of CFS walls with gypsum sheathing under combined axial and lateral loading, where two scenarios of service (the factored dead and live loads that was around 35% of the vertical capacity of the specimens) and design (which corresponds to the highest allowable gravity load that could be applied to the specimens based on the calculated axial capacity) gravity load levels were examined. The results indicate that vertical load plays a valuable role in the shear behavior of this

type of CFS panels. There was no significant deformation under service vertical action in the studs, while buckling of studs occurred in all specimens under vertical action at the design level. However, since the material type of the gypsum wall board is brittle with low tensile to compressive strength ratio, and the maximum tensile stress in the board was significantly reduced by increasing the gravity load level, the board could carry more lateral force due to its compressive resistance. Thus, wall panels under design gravity load could provide higher shear capacity, stiffness and energy absorption, but lower ductility compared to specimens under service vertical action, where the failure has changed from ductile to a brittle one.

CFS structures have been numerically investigated by utilizing various finite element softwares, which give reliable outcomes at a minimal cost comparing with experiment expenses. Nevertheless, the innovative strengthening methods have led to the evolution of new structural configurations and construction materials. However, the numerical analysis of such advanced systems needs great efforts, time, energy, and costs. Thus, developing simplified numerical models is a feasible solution to analyze the complicated performance of advanced systems with less time and effort. Namely, Guan et al. [18] tested CFS floor systems with gypsum slabs, where a theoretical method was proposed to predict the displacement of such arrangements. Based on their findings, they developed a simplified model of the examined CFS floor system in ABAQUS software by using nonlinear diagonal springs to predict the in-plane displacements of such systems, where the in-plane stiffness of the tested floors was characterized by the stiffness of the nonlinear diagonal springs, based on the proposed equivalent in-plane stiffness method. In addition, numerous research works suggested different finite element models by implementing springs instead of some components [19] 20, 21, 22.

Moreover, Martínez-Martínez and Xu [23] proposed a simplified finite element model of CFS panels in order to reduce the time and effort needed to model such type of structures, especially when the overall behavior of the building has to be assessed. The panels consist of studs covered with structural sheathing, and they were modeled using 16-node shell elements in SAP2000, assuming equivalent material properties. Additionally, a stiffness degradation factor was proposed to consider the nonlinear behavior of shear wall panels. The comparison showed good agreement between experimental results and the simplified approach. However, this method has some limitations regarding axial forces, which were larger by 50% than those obtained using conventional finite element analysis.

In this Section, many references have been mentioned and summarized. Most of them were involved in

developing some advanced CFS structural systems to improve the load-bearing resistance and enhance the performance, by mainly tackling the global buckling issue. Many experimental tests were conducted in some studies, while other works were interested in numerical modeling as well as developing some simplified modeling techniques for specific cases. Such as using springs, links, or flat shell elements with equivalent properties to replace some members, complex connection types or even systems with some limitations.

Consequently, this paper suggests a new simplified practical manner for the modeling and simulation of PAC-encased C-profiled CFS wall panels.

### 3 Investigation of PAC-encased CFS wall panels under shear action

In this section, a simplified finite element model of PAC-encased CFS shear wall panels will be developed, and validated according to existing test results, which will be summarized in Sect. 3.1. The test-based design resistance of each specimen will be determined according to Eurocode and compared to the obtained numerical design values. Additionally a parametric study to investigate the effect of PAC properties on both lateral capacity and stiffness of PAC-encased CFS wall panels will be carried out in Sect. 3.5.

### 3.1 Test program

A detailed experimental program [1] was conducted previously to investigate the behavior and resistance of PAC-encased C-profiled CFS shear wall panels. In this test program, both lateral stiffness and ultimate capacity of PAC-filled thin-walled steel panels were examined. Wall panels with 1.8 m width and 2.7 m height were tested without any steel bracing elements; hence, only the concrete provided the shear resistance. The panels were made up of five C140-10 studs and top and bottom tracks with a measured thickness equal to 0.96 mm, where the steel yield stress was 271 MPa. The size of the lips was 13 mm, and the flanges were 41 mm wide for all profiles. The nominal bulk density of the applied PAC-mixture was 200 kg/m<sup>3</sup>, where the values vary between 196 and 227 kg/m<sup>3</sup>. The thickness of PAC was either 400 or 250 mm, depending on the wall type (external or internal). A gap of 50 mm of the concrete cover was performed at both top and bottom ends to establish the connections between testing equipment and specimens that were established by self-drilling screws. The panel arrangement is depicted in Fig. 2. A testing frame that can be used separately for compression and shear tests was built to maintain the required load, where the specimens were placed onto a bearing structure, as shown in Fig. 3. For compression tests, the load was introduced through a hot rolled I-beam attached at the top of the specimen as a load-distributing element, where the load was imposed by two identical hydraulic jacks connected to the same hydraulic circuit, thus producing an equal load. On the other hand, the horizontal force

Fig. 2 Shear panel arrangement of the tested PAC-encased CFS panels [1]

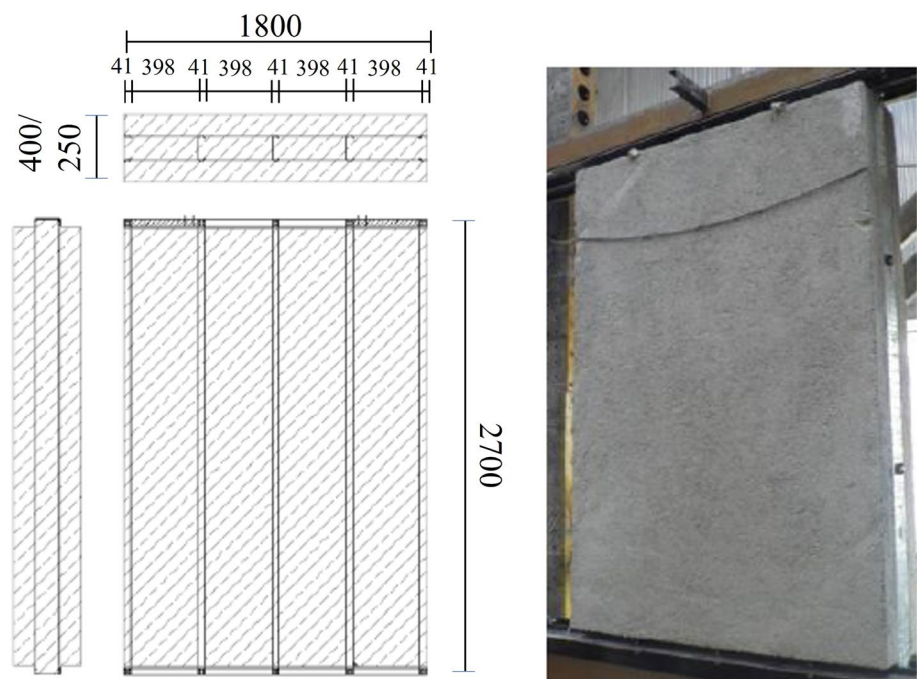
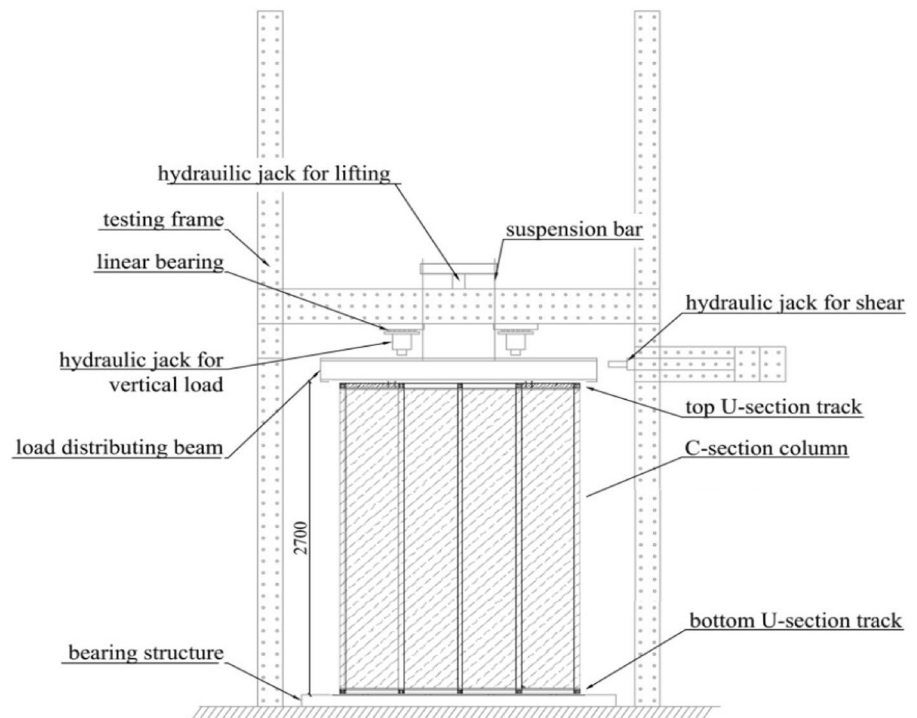


**Fig. 3** Loading frame and build-up of wall panels



in shear tests was applied using a separate hydraulic jack at the end of the load-distributing element. This jack could produce not only compression force but also tension, thus allowing re-adjusting of the panel after lateral loading.

The type of the applied shear load was pulsing in order to test the lateral behavior of full-scale wall panels, where different amplitude impulses were applied to the specimens that were unloaded back to zero load level after specific load intensities. In the final load step, the load was increased above 20, where the panels were loaded until failure. Hence, pulsing shear load means loading and unloading the structure several times in the elastic range until reaching the ultimate load and failure at the last step. Three load intensities were used (8.5 kN, 15 kN and 20 kN, respectively) to investigate the cyclic behavior of the specimens, using three cycles in each load intensity. These intensities are usually defined approximately to be within the elastic behavior of the structure to test several factors such as the serviceability load level, and stiffness degradation. The relative displacement at the top and bottom were measured by inductive transducers. All tests were carried out at the age of 28 days of the concrete. Mainly, two types of failure were detected. The first one was the failure of steel cores, which was observed in the panel with 400 mm thickness, as illustrated in Fig. 4. The failure mechanism was demonstrated by the local buckling of connection zones at the compression side, while it was a failure of screws at the tensile side that occurred at

the peak load level, where also the local buckling deformations at the compression side increased significantly.

The second failure type was a combined failure of steel cores and PAC. Similarly to the first type, local buckling of compressed column-ends has occurred. Eventually, the PAC-block cracked at the web of C-profiles, causing a significant decrement in the load capacity, as shown in Fig. 5. The test results and details of specimens are listed in Table 1.

### 3.2 Numerical model development

ANSYS software [24] was employed to develop a nonlinear finite element model by using the four-node SHELL 181 finite element with reduced integration for CFS elements. 10 mm was the maximum element length in the applied mesh. The elastic modulus ( $E$ ) of steel was 210 GPa, and Poisson's ratio was 0.3. The measured values of yield strength and thickness were used for each specimen according to Table 1. A bilinear material model that is defined as Von-Mises yield criterion with isotropic hardening in the software was implemented here for the steel part. The slope of the plastic part was assumed as  $1/10000$  of  $E$  according to EN 1993-1-5 Annex C [25]. For simulating the self-drilling screws, a two-node beam element in 3-D (BEAM188) that is suitable for linear, large rotation, strain nonlinear applications, and nonlinear material models [24] was used.

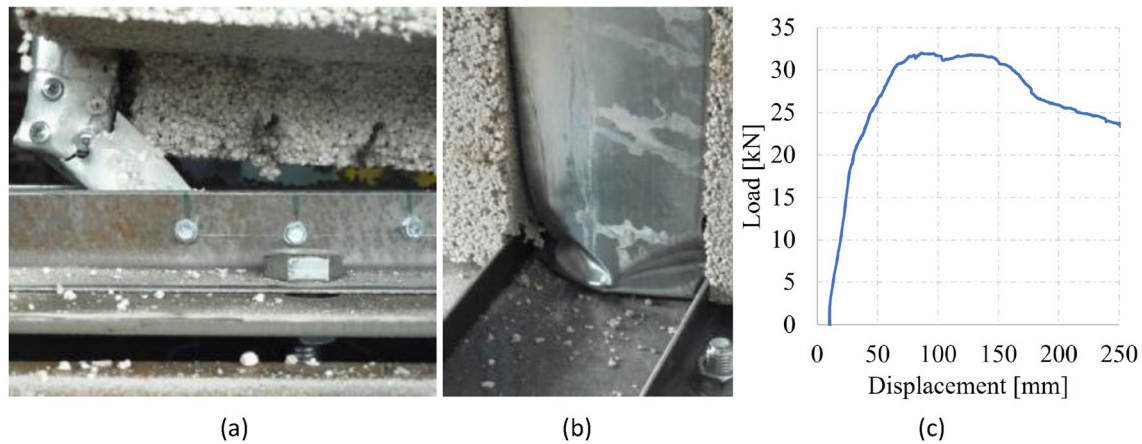


**Fig. 4** Failure of steel cores: **a** on the tension side, **b** on the compression side and **c** load–displacement curve [1]

**Fig. 5** Combined failure: **a** failure shape and **b** load–displacement curve [1]

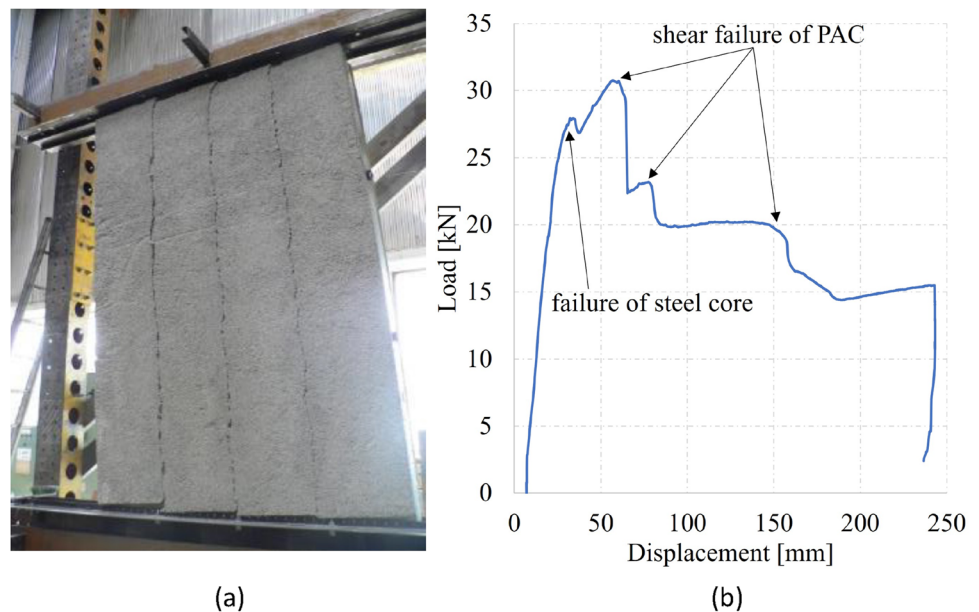


**Table 1** Specimens data and experimental test results. [1]

| Corresponding specimen | Concrete thickness [mm] | Column distance [mm] | Steel nominal thickness [mm] | Steel measured thickness [mm] | Steel Yield strength [MPa] | Ultimate load [kN] |
|------------------------|-------------------------|----------------------|------------------------------|-------------------------------|----------------------------|--------------------|
| C140-10-external       | 400                     | 400                  | 0.9                          | 0.96                          | 271                        | 32.04              |
| C140-10-internal       | 250                     | 400                  | 0.9                          | 0.96                          | 271                        | 30.75              |

To model the contact between tracks and C sections, the line-to-surface contact elements, CONTA177 and TARGE170, were used. While to model the contact between the flanges of U tracks and studs, the surface-to-surface contact elements CONTA174 and TARGE170 were chosen. All contact pairs were identified as frictionless, and the mesh was consistent on both sides.

In fact, the full detailed volume-contact elements-based modeling of PAC-encased specimens is a challenging and time-consuming task. Thus, the main goal of this research study is to develop a simplified finite element model for this new system, where the concrete part can be modeled in an alternative way. Particularly, the exact panel dimensions were modeled using BEAM189



element, which is a quadratic three-node beam element in 3-D; each node has six degrees of freedom. It is based on Timoshenko beam theory, which includes shear-deformation effects, and hence, it is well-suited for large-strain nonlinear applications. The assigned material model was elastic–plastic bilinear, with a nominal plateau slope that was taken as  $E/10,000$ , where  $E$  is the elastic modulus of concrete, which is similar to the real PAC behavior examined in [1]. The used values are detailed in Table 2. This concrete panel represents the global shear stiffness provided by PAC, and it is illustrated as a line in the numerical model, as shown in Fig. 6a. Whereas to provide the local support effect of PAC to the plates, springs were applied at each node of the CFS studs perpendicular to the plate's plane with equivalent properties. COMBIN40 element was employed to represent the springs in the simulation process. It has two nodes with one degree of freedom for each end. The degree of freedom was set to be compatible with the out-of-plane axis of each plate, which was  $U_x$  for the flanges and  $U_z$  for the web in this problem. The stiffness of springs was set using Eq. 1, which was derived within the framework of this research study [3] based on combined analytical [1] and numerical [3] studies, where  $(b/t)$  is the plate width to thickness ratio;  $(E_c)$  is the PAC Young's modulus and  $(A)$  is the element size which can be defined based on the mesh density of steel plates. Based on that, the used stiffness of springs ( $K$ ) range for this case varied between 1 and 150 N/mm, where different values were implemented in each column based on the area supported by each node, as shown in Fig. 7. Blue supports were used to illustrate the springs at each node, where red squares were employed to indicate the different areas supported by each spring with a black cross on the corresponding node.

The theoretical concept behind this idea comes from the buckling resistance of plate elements resting on an elastic foundation, where the effect of encasing material can be considered using an equivalent Winkler-type foundation stiffness that can characterize the restraining effect on the plate buckling behavior. Based on these assumptions, two analytical equations were proposed for predicting the critical stress of internal (Eq. 2) and outstand (Eq. 3) compressed plates resting on an elastic foundation [1].

$$K = -200 \left[ \frac{N}{mm} \right] + 4 \left[ \frac{N}{mm^3} \right] A + 2.5 [mm] E_c + 0.009 \left( -A^2 \left[ \frac{N}{mm^5} \right] + A \cdot E_c \left[ \frac{1}{mm} \right] + E_c^2 \left[ \frac{mm^3}{N} \right] \right) \quad (1)$$

$$\sigma_{cr,p} = 4 \frac{\pi^2 E_s}{12(1 - \nu_s^2)(b/t)^2} - \frac{4680 \text{MPa}}{b/t} + 2.35 E_c + \sqrt{E_c \cdot 3025 \text{MPa}} \quad (2)$$

$$\sigma_{cr,p} = 0.43 \frac{\pi^2 E_s}{12(1 - \nu_s^2)(b/t)^2} + \frac{1200 \text{MPa}}{b/t} + 2.22 E_c + \sqrt{E_c \cdot 3390 \text{MPa}} - 40 \text{MPa} \quad (3)$$

After that, two FE models were developed for internal and outstand plates and implemented into a parametric study with different variables, including  $(b/t)$ ,  $(E_c)$  and  $(A)$ . In each analysis, the stiffness of springs was calibrated such that the critical stress obtained from the linear buckling analysis was the same as the analytical solution of internal (Eq. 2) and outstand (Eq. 3) plates. Eventually, the formula that assumes the value of  $K$  (Eq. 1) was derived based on the numerical data that were obtained from Ansys and by using the incorporated curve fitting tool in MATLAB.

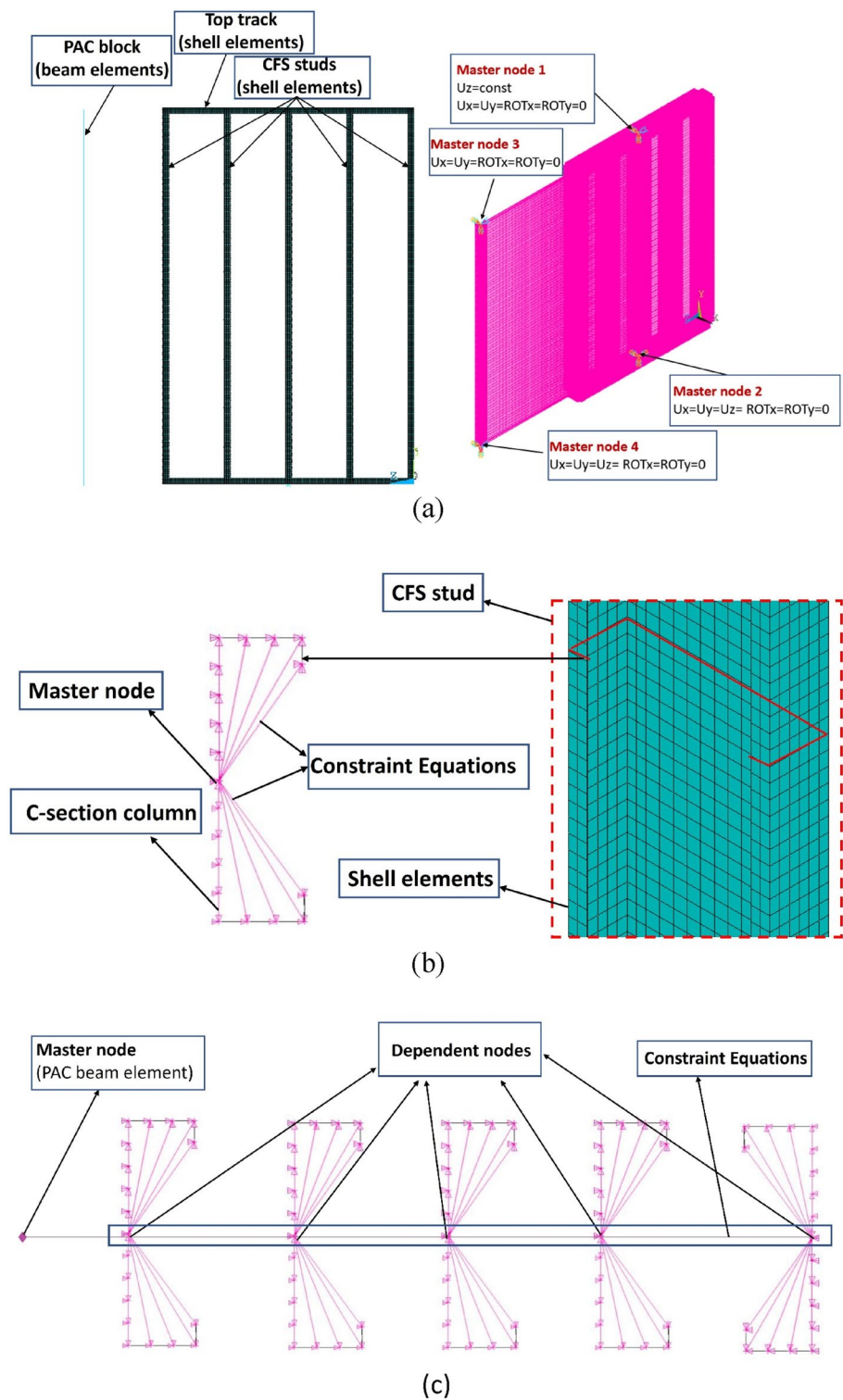
Furthermore, and consistently with the mesh density, rigid regions were defined at each cross-section level, as shown in Fig. 6b. In particular, constraint equations (CE) were generated to relate nodes in each cross-section along the height using the CERIG command, where the node in the middle of the web for each column was set as a master node, as shown in Fig. 6b, and all the applicable degrees of freedom were associated with the equations, which have effect perpendicularly to the plate's plane to provide local support effect. The generated constraint equations are based on the small deflection theory.

Finally, another CE group was defined to connect each cross-section along the height of columns to the global shear stiffness line, where the master nodes of columns were connected at each longitudinal level to the same level node from the PAC beam elements, which was set as an independent node, as detailed in Fig. 6c, where all the applicable degrees of freedom were associated with the equations. Consequently, the combination of local and global stiffness of PAC could produce the actual shear behavior of PAC-filled wall panels.

**Table 2** PAC properties and comparison of tests and FEA peak loads

| Corresponding specimens | Concrete thickness [mm] | $E_c$ [MPa] | $f_c$ [MPa] | Ultimate load [kN] |             |                        |
|-------------------------|-------------------------|-------------|-------------|--------------------|-------------|------------------------|
|                         |                         |             |             | $F_{u,test}$       | $F_{u,num}$ | $F_{u,num}/F_{u,test}$ |
| C140-10-external        | 400                     | 20          | 0.12        | 32.04              | 32.55       | 1.02                   |
| C140-10-internal        | 250                     | 40          | 0.18        | 30.75              | 30.91       | 1.01                   |

**Fig. 6** Applied boundary conditions and details for the developed numerical model: **a** 3D view (right) and elevation view (left), **b** CE layout for the studs and **c** top view with the layout of the second CE group



The boundary conditions were pinned at the bottom and simply supported at the top for both tracks and the column that represents the concrete part. The nodes of the tracks were connected through rigid regions to a master node in the middle, where the boundary conditions

were applied. For the pinned ends, the rotations about the maximum inertia axis were permitted, while the three translations, rotation along the longitudinal axis of the profile, and rotation around the minor inertia axis were all restricted. Likewise, rotations around the longitudinal

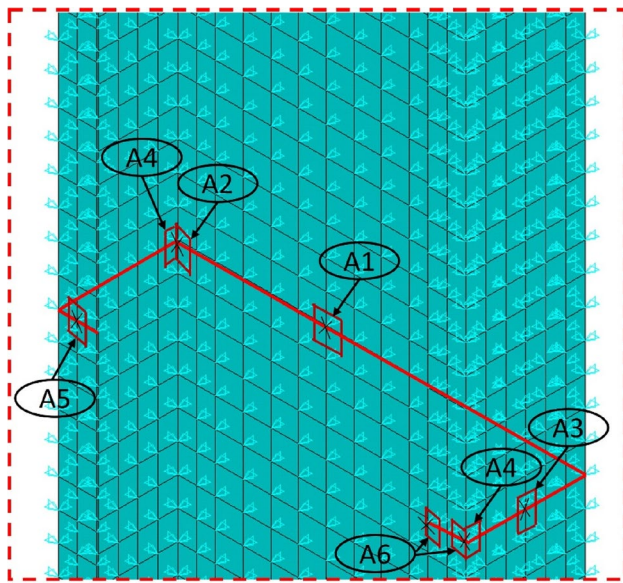


Fig. 7 The layout of springs with the area supported by each node

profile axis and the minor inertia axis were all restrained for the simply supported ends, while rotations about the Z axis were permitted. Although pulsing loading was applied during tests, a nonlinear pushover analysis was carried out, where monotonic pushover loading was imposed using ANSYS software. In particular, translation in the horizontal direction was imposed at the master node of the top track (master node 1), as illustrated in Fig. 6a.

The main two buckling modes, which were obtained by performing linear buckling analysis, have been tried out with different imperfection amplitudes. However, the results showed that the applied modes and amplitudes do not have an impact on the lateral capacity, especially that the resistance was provided mainly from the concrete contribution part. Therefore, the imperfection amplitude  $b/200$ , where  $b$  is the plate width, was used according to Eurocode recommendations [2]. Examples of the two buckling modes for the side column are shown in Fig. 8.

Fig. 8 The main two buckling modes

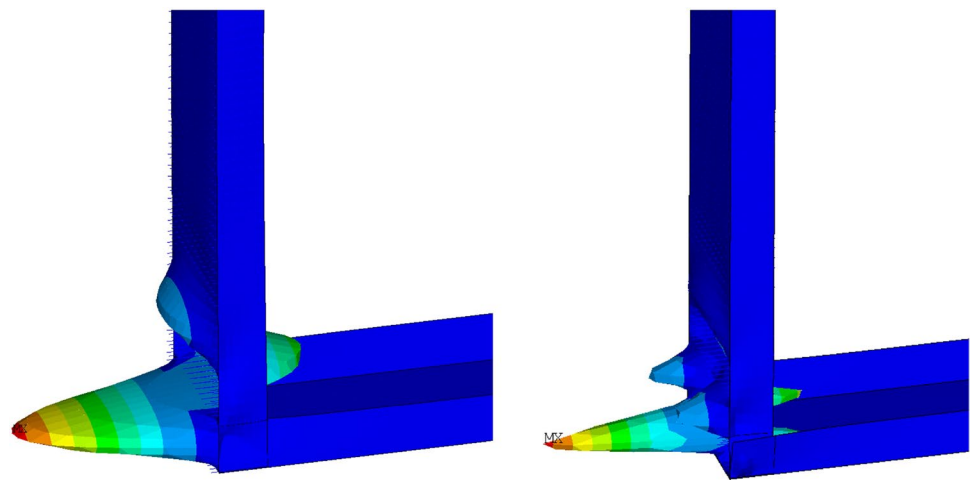
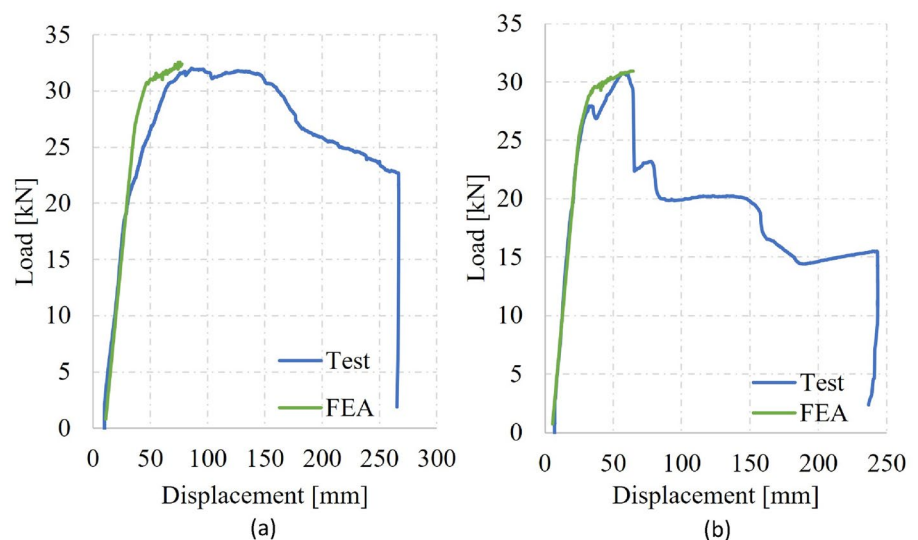


Fig. 9 Numerical and experimental load–displacement curves of the encased C140-10 **a** external and **b** internal panel



Finally, GMNI analysis was carried out, and the Newton–Raphson algorithm was implemented to solve the problem. To validate the model, finite element and experimental results were compared in Fig. 9a for external walls and Fig. 9b for internal walls, showing good agreement regarding stiffness and ultimate resistance. However, the post-peak branch could not progress due to the high nonlinearity in the problem, which has led to some numerical and convergence issues beyond the peak value. Additionally, for internal walls, it is not feasible to get the same jumps in the load–displacement curve that occurred because of the developed cracks along the whole thickness of PAC at each column position due to the use of implicit numerical analysis in case of both simplified and full detailed volume-shell models. Thus, the proposed FE model cannot simulate the separation in the concrete panel and, hence, reproduce the jumps in the post-peak branch for internal walls. The values for both tests and numerical analyses are listed in Table 2. Comparisons of the side column failure modes are shown in Figs. 10 and 11. The simulation outcomes showed that both PAC and

steel govern the failure; however, linear material model of PAC was implemented to avoid the nonlinear yielding failure of the PAC material and to be able to show the steel failure modes with large plastic deformation and prove that the model is capable of the failure modes. Nevertheless, further research work is needed to improve the PAC failure by modeling the separation in the concrete panel and using improved nonlinear material model for the concrete.

### 3.3 Step-by-step design guide for the application of the proposed simplified model

In this part, practical steps are listed below to be followed during the simulation of PAC-encased CFS wall panels according to the proposed modeling methodology.

1. Creating a shell model for the core (CFS) studs and tracks.

**Fig. 10** Comparison of the failure of the side column between the test [1] and FEA

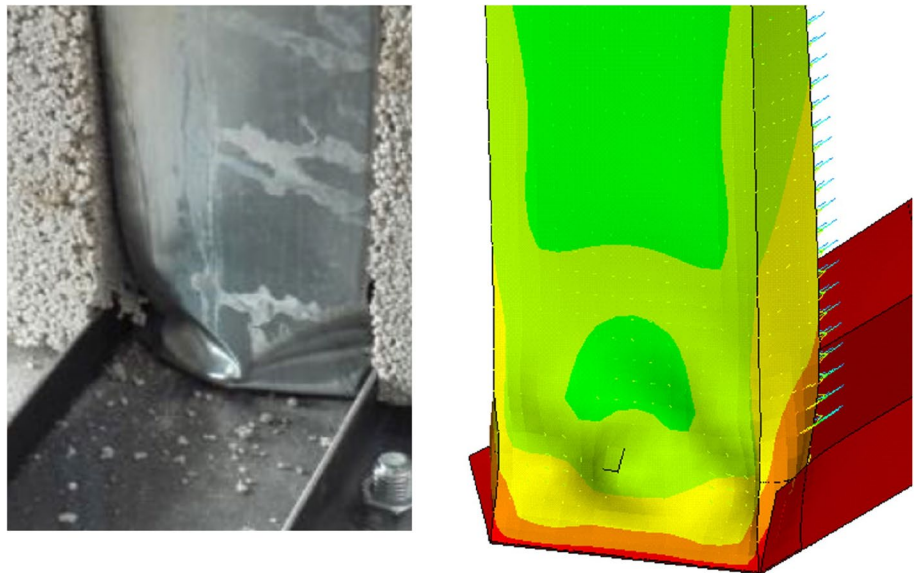
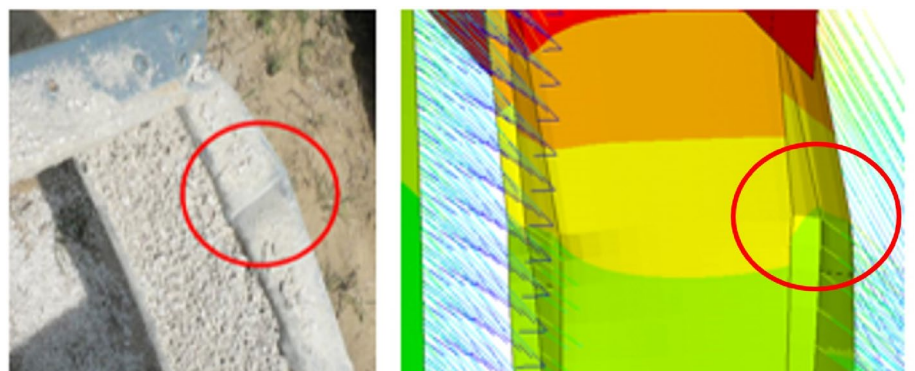


**Fig. 11** Comparison of the buckling shape near the column-end between the test [1] and FEA



2. Determining the stiffness of springs according to Eq. (1) based on the elastic modulus of the filling material and the element size of the FEM model.
3. Creating spring elements along the studs as a replacement for the filling material.
4. Connecting all the springs for each column at each elevation according to the mesh density by generating constraint equations, where the node in the middle of the web of each cross-section level can be set as a master node.
5. Creating a column representing the concrete panel with the same height and dimensions using a beam element type with an appropriate material model, like the real behavior of the filling material. This concrete panel represents the global shear stiffness provided by PAC.
6. Connecting all the parts of the model by creating constraint equations along the height, based on the mesh density, between the PAC beam column and the master nodes of the constraint equations from step 4. In this case, the nodes of the PAC beam column can be set as independent nodes.
7. Applying equivalent imperfections according to the recommended shape and amplitude.
8. Defining nonlinear material type for the steel core and PAC beam elements and running the GMNI analysis.

### 3.4 Design resistance calculation for encased specimens

There are some books and codes that explain the structural behavior and specify the design rules of CFS structures, such as the American Iron and Steel Institute standard (AISI S100-16) [26], Australia and New Zealand code (AS/NZS 4600:2018) [27] and Eurocode 3 Part 1–3 (EC3-1-3:2006) [2]. Two main methods are used in determining the capacity of CFS elements according to the available standards. The first one is the effective width method that estimates the effect of local plate buckling. The second one is the direct strength method, which can directly assess the capacity of a member based on specific buckling curves. However, the current design rules are not applicable to all configurations and connection types; thus, the test-based design approach allows the

calculation of design resistances for specific tests that are measured in laboratories and still provides the necessary safety level for design purposes. Additionally, the development of the actual design methods in standards can be done based on the observations of test-based design calculations, where nonconservative design methods may be derived and consequently reduce the construction cost of structures. In this research work, test-based design values of PAC-encased CFS shear wall panels were computed in accordance with EC 1993-1-3 2006 [2] as follows:

Based on the measured test outcome  $R_{obs}$  and taking into account the discrepancy between measured and nominal parameters, the adjusted resistance  $R_{adj}$  of the experimental results was defined in the first stage according to EC 1993–1-3 2006 (A.6.2) [2]. For the test with steel core failure (external wall), the steel properties were substituted into Eq. (5). In contrast, the concrete properties were implemented in the calculations for combined failure (internal wall) since the peak load has been developed due to the shear failure of PAC.

$$R_{adj,i} = \frac{R_{obs,i}}{\mu_R} \tag{4}$$

In which  $\mu_R$  is the adjustment coefficient:

$$\mu_R = \left( \frac{f_{yb,obs}}{f_{yb}} \right)^\alpha \left( \frac{t_{obs,cor}}{t_{cor}} \right)^\beta \tag{5}$$

$\alpha$  is an exponent that can be obtained as follows:

- if  $f_{yb,obs} \leq f_{yb} : \alpha = 0$
- if  $f_{yb,obs} > f_{yb} : \alpha = 1$

where  $f_{yb,obs}$  : the measured yield strength, as listed in Table 3.

$f_{yb}$ : the nominal yield strength, that was assumed as 275 MPa for the used steel material; based on [1], in the calculation of the external wall resistance. For the internal wall and according to the specifications of EN 1990 [28], the 0.1% quantile value should be used for determining design values for material properties. By defining the suitable distribution of the measured data of PAC

**Table 3** Test based design calculations of the tested PAC-encased CFS shear wall panels

| Corresponding specimens | Measured values |                    |                  | Adjusted resistances |         |         |                  | Design resistances |            |
|-------------------------|-----------------|--------------------|------------------|----------------------|---------|---------|------------------|--------------------|------------|
|                         | $t_{obs}$ [mm]  | $f_{yb,obs}$ [MPa] | $R_{obs,i}$ [kN] | $\alpha$             | $\beta$ | $\mu_R$ | $R_{adj,i}$ [kN] | $R_k$ [kN]         | $R_d$ [kN] |
| C140-10-external        | 0.96            | 271                | 32.04            | 0                    | 2       | 1.14    | 28.16            | 22.81              | 22.81      |
| C140-10-internal        | 250             | 0.18               | 30.75            | 1                    | 1       | 2.00    | 15.38            | 12.45              | 12.45      |

strength from regression analysis, the design concrete strength value was 0.09 MPa.

$\beta$  is an exponent that should be taken as follows:

- if  $t_{obs,cor} \leq t_{cor}$ :  $\beta = 1$
- if  $t_{obs,cor} > t_{cor}$ : if  $b_p/t \leq (b_p/t)_{lim}$ ,  $\beta = 1$ ; if  $b_p/t > 1.5(b_p/t)_{lim}$ ,  $\beta = 2$ , where:

$$(b_p/t)_{lim} = 0.64 \sqrt{\frac{Ek_\sigma}{f_{yb}}} * \sqrt{\frac{f_{yb}/\gamma_{M1}}{\sigma_{com,Ed}}} \tag{6}$$

where  $\sigma_{com,Ed}$  is the largest compressive stress in the member ( $\sigma_{com,Ed} = f_{yb}$ ),  $k_\sigma$  is the buckling factor and  $b_p$  is the notional flat width.

$t_{obs,cor}$ : the measured thickness, as listed in Table 3.

$t_{cor}$ : the nominal thickness, it was equal to 0.9 mm; for the steel, in the calculation of the external wall capacity, and 250 mm; for PAC, in the calculation of the internal wall capacity.

In the next stage, the adjusted test result  $R_{adj}$  should be used to determine the characteristic resistance, as there was just one test performed for each situation in this test program, the associated characteristic resistance was defined according to EC 1993-1-3 2006 (A.6.3.3) [2], using the following equation:

$$R_k = 0.9\eta_k R_{adj} \tag{7}$$

$\eta_k$  can be determined based on the failure mode as follows:

Gross deformation:  $\eta_k = 0.9$ , yielding failure:  $\eta_k = 0.9$ , local buckling:  $\eta_k = 0.8 \dots 0.9$  according to the effects of global behavior in tests, overall instability:  $\eta_k = 0.7$ . Since no global deformation was detected during tests; where no global buckling occurred due to the PAC supporting effect, the value 0.9 was adopted in the calculation.

Finally, based on the characteristic value  $R_k$ , the design resistance  $R_d$  was determined for each test as specified in Table 3, according to EC 1993-1-3 2006 (A.6.4) [2] using:

$$R_d = \eta_{sys} \frac{R_k}{\gamma_m} \tag{8}$$

$\gamma_m$ : is the partial factor for resistance; (1 for buildings).

$\eta_{sys}$ : is a conversion factor for differences in behavior under experimental and service conditions. (It was assumed as 1 in the calculation).

Furthermore, numerical design values were obtained by using the same nominal and design parameters, which were used in the calculation of test-based design values in the developed numerical model, where a comparison between test-based design capacities and numerical design values is detailed in Table 4.

**Table 4** Comparison of design values of the tested PAC-encased CFS shear wall panels

| Corresponding specimens | Design resistances [kN] |             |                        |
|-------------------------|-------------------------|-------------|------------------------|
|                         | $F_{d,test}$            | $F_{d,num}$ | $F_{d,num}/F_{d,test}$ |
| C140-10 external        | 22.81                   | 23.44       | 1.03                   |
| C140-10 internal        | 12.45                   | 13.49       | 1.08                   |

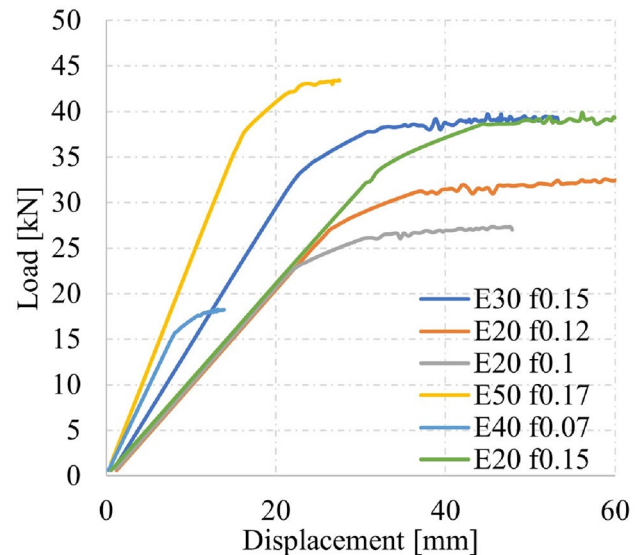


**Fig. 12** Parametric study of PAC properties

### 3.5 Parametric study of PAC properties

Different values for  $E_c$  [20–50] MPa and  $f_c$  [0.07–0.17] MPa were implemented into this study, which is illustrated by load–displacement curves in Fig. 12. The curves show that the same elastic modulus with different strengths of PAC gave the same stiffness, as represented by the green, red and grey curves. Furthermore, the exact capacity has been achieved using the same  $f_c$  as represented by the blue and green curves. It can also be concluded from the results that both stiffness and resistance capacity has increased linearly with the increment of  $E_c$  and  $f_c$ , respectively.

In this Section, a numerical study was presented in which a guideline to model PAC-encased cold-formed steel elements subjected to shear load was proposed. Design values were evaluated, and the influence of the concrete properties on the lateral structural performance was assessed through a parametric study.

In the next Section, the structural behavior under combined action of compression and shear will be examined numerically using the verified FE model to get design values, where an interaction curve was proposed. The Section will also include a sensitivity study to explore the effect of vertical load eccentricity, which may occur in practice on the axial resistance.

#### 4 Investigation of wall panels under combined vertical and shear loading

In this section, the structural performance of PAC-encased CFS panels under combined vertical and shear loading was examined, where the effect of different axial load levels on the lateral strength and stiffness of PAC-encased CFS walls was determined, and an interaction equation was proposed. The behavior of the investigated PAC-encased CFS shear panels in Sect. 3 was investigated in this section under combined vertical and shear loading. The FE modeling techniques defined in Sect. 3.2 for external walls were replicated herein to evaluate the effect of gravity load on the performance of the examined shear wall panels. The loading procedure was performed in two steps. In the first stage, the vertical load was applied, with a specific ratio of the design compressive capacity that was obtained by implementing nominal dimensions and material properties in the FE model. In the second phase, the shear load was imposed until failure. The outcomes were evaluated in terms of load capacities, failure shapes, initial stiffnesses, and load–displacement curves.

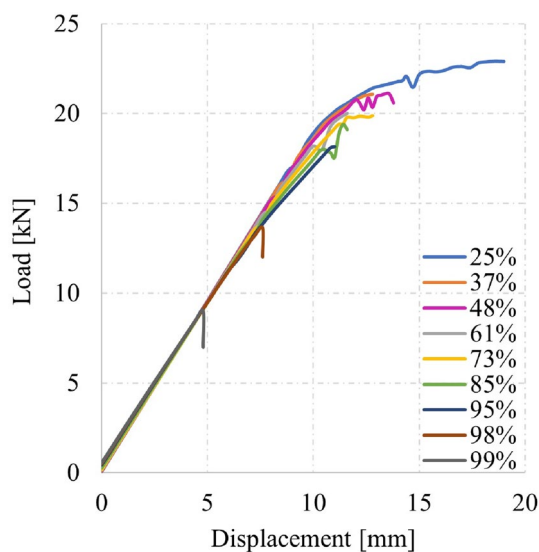


**Fig. 13** Lateral load–displacement curves with various gravity load levels

The lateral capacity has been slightly affected by vertical loads of up to 95% of the compressive design capacity of encased panels, where it was decreased by 22%, as illustrated in Fig. 13. Nevertheless, vertical load with intensity levels higher than 95% of the compressive design capacity of the analyzed panel was able to reduce the lateral strength of the panel by more than 60%. Besides, the influence of gravity loads on the initial stiffness of the system was shown to be minimal. These consequences can be explained by the fact that the lateral stiffness and resistance come principally from the concrete contribution part that remained in the elastic range without any visible damage under pure compression tests.

Thereafter, by implementing a manual optimization method, a general binomial expansion was proposed for the interaction equation. This was achieved by avoiding unsafe and excessively conservative cases simultaneously and using a similar interaction equation form as suggested by current design specifications to provide a well-comprehensible and easily applicable equation for engineering practices. The difference between the capacities obtained from FE models and the predicted values were set to be as minimal as possible, providing that the safety conditions are met and, hence, the following interaction expression was proposed to predict the resistance of PAC-filled CFS wall panels subjected to combined action of axial  $N_{Ed}$  and shear  $V_{Ed}$  force, with an acceptable tolerance:

$$\left(\frac{V_{Ed}}{V_{Rd}}\right)^3 + 0.97\left(\frac{N_{Ed}}{N_{Rd}}\right)^{1.5} \leq 1 \quad (9)$$

where  $V_{Rd}$  is the design shear resistance of PAC-encased CFS panels that can be obtained from FE analyses by using nominal dimensions and material properties under pure shear force.

$N_{Rd}$  is the design axial resistance of the PAC-encased CFS panels obtained from FE analyses by using nominal dimensions and material properties under pure axial force.

The numerical results and the proposed interaction curve are presented in Fig. 14, along with the failure mode of some cases. When the dominant force was compression, a classical connection failure occurred, which is a kind of local buckling at the end part of the studs. In comparison, a sort of local and distortional interaction buckling was detected in the other cases.

Lastly, a sensitivity study of the effect of vertical load eccentricity, which may occur in practice, was conducted. The applied eccentricity range was between  $b/14$  and  $b/5$ , where  $b$  is the web width. The eccentricity was applied in the X direction, which is parallel to the out-of-plane axis of the panel. The results indicate that the axial capacity could be reduced by up to 28%, depending on the applied eccentricity. Additionally, the observed failure mode for this case

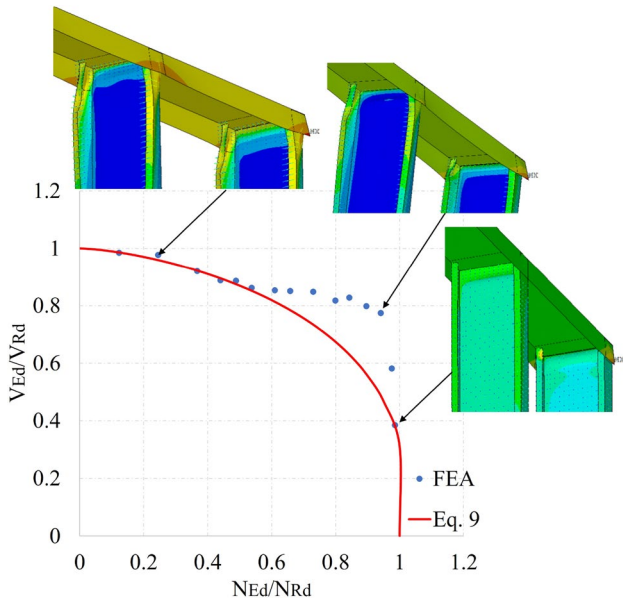


**Fig. 14** Interaction evaluation of  $V_{Ed}/V_{Rd}$  and  $N_{Ed}/N_{Rd}$  according to FEA and the proposed design interaction curve

was an asymmetric buckling mode of the connection failure of the top part of studs consistent with the load application side, as depicted in Fig. 15.

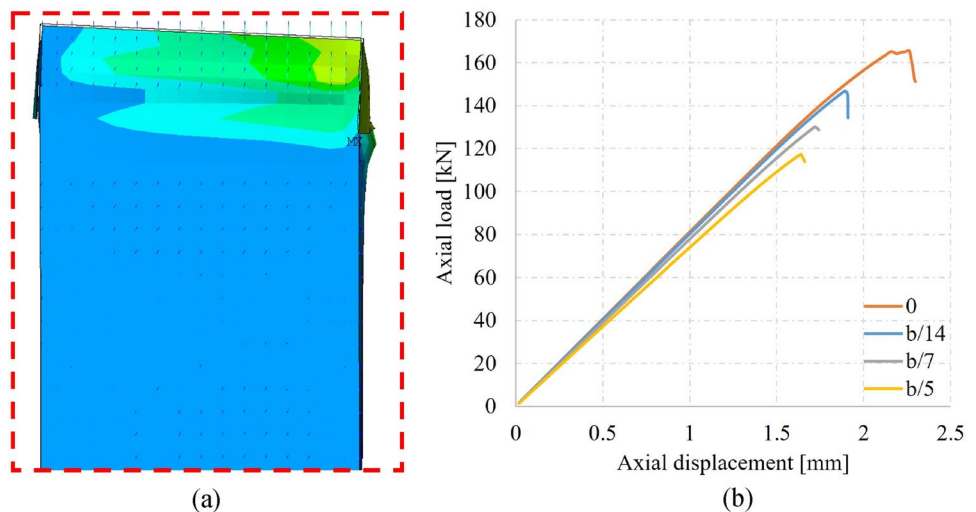
### 5 Conclusions

A simplified numerical model approach was developed for PAC-encased CFS shear walls, considering geometric nonlinearity, nonlinear material properties and geometric imperfections. The models were validated against available experimental results regarding load–displacement curves and failure modes. Based on this modeling

technique, a comprehensive parametric study was conducted to determine the effect of PAC material properties on the lateral resistance and stiffness of the examined specimens, and the behavior under combined loading of vertical and shear was assessed. To sum up, the following conclusions could be derived from this paper:

- The model of PAC-encased CFS shear wall panels was performed with a developed modeling technique that can simulate the concrete part more accurately, especially that the concrete plays a significant role in providing the shear resistance in such structures.
- The developed model is proved to have appropriate accuracy and efficiency for simulating the behavior of PAC-encased C-profiled CFS shear wall panels by validating the model with the available tests.
- The innovative, simplified finite element model (shell, beam and spring elements with constraint equations), which separates the local and global behavior, can be used efficiently to simulate the structural behavior of PAC-encased CFS wall panels of C90 and C140 profiles with thicknesses less than 1.5 mm.
- The efficacy and validity of the developed modeling technique have been checked for PAC-braced CFS wall panels under compression action, where the previously performed models for similar panels were replicated using the new modeling technique. The results revealed that both methods gave the exact results; hence, the developed shear modeling technique can be used successfully for shear and compression loading as well.
- The parametric study of PAC properties in the shear case has concluded that the PAC properties have a considerable effect on the lateral performance of PAC-encased CFS wall panels since it is the main resistance component of this system for shear loads. At the

**Fig. 15** Sensitivity study on the effect of vertical load eccentricity: **a** asymmetric failure mode and **b** axial load- displacement curves





same time, the imperfection amplitude, along with the stiffness of springs, have a minor effect on the lateral behavior in this system.

- The interaction of axial and shear loading was examined through numerical analyses. The results showed that the effect of axial force on the lateral capacity of encased CFS panels is minor when the axial load level is less than the maximum axial resistance of the analyzed panel by 5%; however, the lateral capacity has dropped by more than 60% when the axial load level exceeds 95% of the compressive design capacity of encased panels. Additionally, a V–N interaction expression was proposed that can assess the resistance of PAC-encased CFS panels under combined action of axial and shear force and gives reasonable results.

Future research work is needed in terms of conducting further experimental tests in order to investigate the structural behavior of more complex cases. Numerical investigation for members under pure bending and the modeling of a two-story building system that can precisely simulate the actual behavior and stiffness of the whole structure will also be performed in the next step of this research.

Consequently, the verified numerical model can be used later to extend the range of the available results by conducting virtual tests for various cross-sections, load combinations, and eccentricities. Subsequently, new experimental testing programs can be designed to define the extreme in the section sizes and load types and perform some of these tests that help to interpolate new outcomes between extreme cases and the available results, and hence the applicability of the developed numerical model can be proved for the extended range. Based on these suggestions, developing proper design provisions and defining interaction curves and design resistances for various load combinations that can be part of the enhanced design specifications in codes can be considered for later research studies.

**Author contributions** Nathalie Eid: Conceptualization, Methodology, Software, Validation, Writing - Original Draft, Visualization. Attila László Joó: Supervision, Writing - Review & Editing, Conceptualization. All authors reviewed the manuscript.

**Funding** The authors have not disclosed any funding.

**Data availability** All data generated or analyzed during this study are included in this published article.

## Declarations

**Competing interests** The authors declare no competing interests.

**Open Access** This article is licensed under a Creative Commons Attribution 4.0 International License, which permits use, sharing, adaptation, distribution and reproduction in any medium or format, as long as you give appropriate credit to the original author(s) and the source, provide a link to the Creative Commons licence, and indicate if changes were made. The images or other third party material in this article are included in the article's Creative Commons licence, unless indicated otherwise in a credit line to the material. If material is not included in the article's Creative Commons licence and your intended use is not permitted by statutory regulation or exceeds the permitted use, you will need to obtain permission directly from the copyright holder. To view a copy of this licence, visit <http://creativecommons.org/licenses/by/4.0/>.

## References

1. Hegyi P (2017) Behaviour and design of C-profiled steel cold-formed structural elements encased in ultra-lightweight concrete. Dissertation, Budapest University of Technology and Economics.
2. EN 1993-1-3, Eurocode 3 (2006) Design of steel structures, Part 1–3: general rules, supplementary rules for cold-formed members and sheeting. Brussels. CEN
3. Eid N, Joó AL (2022) Simplified numerical model development for advanced design of lightweight-concrete encased cold-formed steel compressed elements. *Adv Civ Eng*. <https://doi.org/10.1155/2022/1207885>
4. Eid N, Joó AL (2022) Simplified numerical model development of lightweight-concrete encased cold-formed steel column-end joints and panels. *ce/Papers* 5(4):170–177. <https://doi.org/10.1002/cepa.1742>
5. Zhang W, Xu X, Liu Y, Yu C, Liu X, Xie Z (2021) High-strength cold-formed steel framed shear wall with steel sheet sheathing. *Thin-Walled Struct* 162:107584. <https://doi.org/10.1016/j.tws.2021.107584>
6. Attari NK, Alizadeh S, Hadidi S (2016) Investigation of CFS shear walls with one and two-sided steel sheathing. *J Constr Steel Res* 122:292–307. <https://doi.org/10.1016/j.jcsr.2016.03.025>
7. Xu Z, Chen Z, Osman BH, Yang S (2018) Seismic performance of high-strength lightweight foamed concrete-filled cold-formed steel shear walls. *J Constr Steel Res* 143:148–161. <https://doi.org/10.1016/j.jcsr.2017.12.027>
8. Chen Z, Sun H, Cao B (2021) Experimental study on seismic behavior of cold-formed steel shear walls with reinforced plastered straw-bale sheathing. *Thin-Walled Struct* 169:108303. <https://doi.org/10.1016/j.tws.2021.108303>
9. Wu H, Sui L, Wang J, Zhou T (2020) Cycle performance tests and numerical modeling of infilled CFS shear walls. *J Constr Steel Res* 168:106010. <https://doi.org/10.1016/j.jcsr.2020.106010>
10. Wu H, Sui L, Zhou T, Lu L, Li X (2021) Estimation of lateral stiffness for gypsum-filled cold-formed steel shear walls. *Structures* 32:28–37. <https://doi.org/10.1016/j.istruc.2021.02.067>
11. Wang W, Wang J, Yang TY, Guo L, Song H (2020) Experimental testing and analytical modeling of CFS shear walls filled with LPM. *Structures* 27:917–933. <https://doi.org/10.1016/j.istruc.2020.06.016>
12. Hu S, Zhou L, Huang Y (2023) Experimental investigation on the seismic performance of phosphogypsum-filled cold-formed thin-walled steel composite walls. *Thin-Walled Struct* 186:110664. <https://doi.org/10.1016/j.tws.2023.110664>
13. Yin C, Zhou L, Zou Q, Xu Y (2022) Effect of filling phosphogypsum on the axial compression behavior of cold-formed thin-walled steel walls. *Buildings* 12(9):1325. <https://doi.org/10.3390/buildings12091325>

14. Usefi N, Ronagh H, Sharafi P (2020) Lateral performance of a new hybrid CFS shear wall panel for mid-rise construction. *J Constr Steel Res* 168:106000. <https://doi.org/10.1016/j.jcsr.2020.106000>
15. Yilmaz F, Mojtabaei SM, Hajirasouliha I, Becque J (2023) Behaviour and performance of OSB-sheathed cold-formed steel stud wall panels under combined vertical and seismic loading. *Thin-Walled Struct* 183:110419. <https://doi.org/10.1016/j.tws.2022.110419>
16. Papargyriou I, Hajirasouliha I (2021) More efficient design of CFS strap-braced frames under vertical and seismic loading. *J Constr Steel Res* 185:106886. <https://doi.org/10.1016/j.jcsr.2021.106886>
17. Ayatollahi SR, Usefi N, Ronagh H, Izadinia M, Javaheri MR (2020) Performance of gypsum sheathed CFS panels under combined lateral and gravity loading. *J Constr Steel Res* 170:106125. <https://doi.org/10.1016/j.jcsr.2020.106125>
18. Guan Y, Zhou X, Shi Y, Yao X (2019) Prediction of the in-plane mid-span displacement of cold-formed steel floor with steel form-deck and gypsum-based self-leveling underlayment. *J Constr Steel Res* 160:124–135. <https://doi.org/10.1016/j.jcsr.2019.03.001>
19. Jeong SH, Jang WS (2016) Modeling of RC shear walls using shear spring and fiber elements for seismic performance assessment. *J Vibroeng.* 18(2):1052–1059. <https://doi.org/10.21595/jve.2015.16757>
20. Wang T, Zhou M, Li Y, Yu Y, He H (2020) Lattice spring model with angle spring and its application in fracture simulation of elastic brittle materials. *Theor Appl Fract Mech.* <https://doi.org/10.1016/j.tafmec.2019.102469>
21. Moshirabadi S, Soltani M (2019) Implementation of smeared crack approach in rigid block and spring modeling of reinforced concrete. *Eng Struct* 201:1–17. <https://doi.org/10.1016/j.engstruct.2019.109779>
22. Selvaraj S, Madhavan M (2019) Bracing effect of sheathing in point-symmetric cold-formed steel flexural members. *J Constr Steel Res* 157:450–462. <https://doi.org/10.1016/j.jcsr.2019.02.037>
23. Martínez-Martínez J, Xu L (2011) Simplified nonlinear finite element analysis of buildings with CFS shear wall panels. *J Constr Steel Res* 67(4):565–575. <https://doi.org/10.1016/j.jcsr.2010.12.005>
24. ANSYS@Academic Research, Release (2023) R1, Help System. Guide, ANSYS Inc, Structural Analysis
25. EN 1993-1-5, Eurocode 3 (2006) Design of steel structures, Part 1-5: plated structural elements. Bruxelles. CEN
26. American Iron and Steel Institute (AISI) (2016) North American specification for the design of cold-formed steel structural members
27. Cold-formed steel structures AS/NZS 4600 (2018) Standards Australia/Standards New Zealand
28. EN (1990) Eurocode (2002) Basis of structural design. CEN, Brussels

**Publisher's Note** Springer Nature remains neutral with regard to jurisdictional claims in published maps and institutional affiliations.